ISABE-2011-1616

SEPARATION OF GEOMETRICAL- AND DEFECT INFORMATION IN DIGITAL RADIOGRAPHS USING WAVELET FILTER TECHNIQUES

Erik Lindgren, Håkan Wirdelius
Department of Materials and Manufacturing Technology, Chalmers University, Sweden

Abstract

This paper describes the development of a mathematical model of new digital x-ray technologies and is part of a project that intends to develop an automated system for structural integrity assessment. The first part of this paper explains the exploited attenuation model based on a ray tracing assumption with piecewise linear attenuation coefficients. This is followed by a description of how the modeled volume is defined by specification of simple mathematical surfaces and the third part specifies typical welds addressed in this project. The model of a digital x-ray detector and its implementation into a simulation tool is thereafter briefly described. A thorough validation of the x-ray attenuation and the simulation software using another software PENELOPE has been conducted. The paper is concluded with an example of intended approach to remove geometrical large scale information by applying wavelet transform of the radiograph.

Introduction

The future of aero industry will be characterized by demands for increased safety combined with increasing fuel costs and emission requirements. The development towards light weight constructions unavoidable implies higher quality demands on used components and less margins for accepted defects. Both cost and sustainable development leads to challenges when it comes to extending expected life time on critical components and at the same time raise the safety margins.

This work attempts to address this need by taking the initial steps towards a methodology that incorporates Nondestructive Evaluation (NDE) and structural integrity together with lifetime assessment. This new area of research, Integrity and quality assessment by NDE (IqNDE), intents to increase the amount of information in the output of nondestructive techniques in order to increase the economic value of the inspections.

The focus of this project is towards integrity assessment of laser welded components in thin titanium plates, a critical component of an aero gas turbine engine. Individual pores with characteristic size of 50-100 micrometer can be detected with recently developed digital x-ray systems. Each of these being of non-critical size but due to their tendency to be clustered (chain porosities) they can have an impact on the structural integrity of the component due to their orientations and relative distances. To handle this in a production line, a computerized and automated evaluation will be needed.

A mathematical model that enables simulation of a number of commercially available digital radiographic NDT systems has been deduced. The model is based on the assumption that the attenuation of photons is mainly by photoelectric absorption. Attenuation due to scattering, e.g. Compton- and Rayleigh scattering, has been simulated by the software PENELOPE[1].

A radiograph typically contains more information than can be visualized in one single presentation (picture). Using gray scales, a human operator can only distinguish a limited number of gray levels[2] in each picture. If the component has a large variation in thickness, the defect indications tends to drown in geometry variations in the radiograph. This is usually addressed by manually adjusting brightness and contrast which is a rather time consuming procedure. Also for computerized defect detection it is favorable to remove as much information of noninterest as possible, i.e. coarse scale geometry in this case. One essential part of this project is therefore to find a filtering technique that withdraws geometrical large scale variations leaving only the defect and noise variations[3]. A wavelet transformation method[4,5] has been described in this paper together with an example of application as an approach to this problem.

X-ray attenuation model

The addressed problem is initially separated into two main tasks, attenuation and geometry handling. The attenuation of the x-rays is approximated[6,3] to follow exponential decay according to

$$\frac{I}{I_0} = e^{-l\mu},$$

where I and I_0 denote intensity with and without the attenuating body in the ray path of length l. The linear attenuation μ is set to constant. The effect of the source's bremsstrahlung spectra[7] is believed to mainly lead to an effective linear attenuation coefficient which is a function of thickness. Under the presumption (validity range) that the change in attenuation coefficient due to geometrical variations in modeled components are small, this effect can be disregarded. The source is modeled as a point source with uniform intensity in all directions which leads to the usual inverse square law scaling of the intensity. A 2D intensity matrix INTENS[i,j] of size DET_N x SUBPXL in each dimension i and j, is then given some physical size defined by maximum and minimum coordinates of the detector. For each element ij, a photon ray is sent out from the point source in a straight line direction. Typically the ray will cross several different bodies k, with a predefined attenuation coefficient μ_k. The resulting expression for the relative intensities then becomes

$$INTENS[i,j] = \frac{e^{\sum_k \mu_k l_k}}{l_{ij}^2}, \qquad (1)$$

where l_{ij} is the distance from the source to intensity indices ij. The above expression will be referred to as the linear attenuation model. The length scale of each element in INTENS should be kept less than the smallest variation of interest in the scene, e.g. defect size, by changing SUBPXL.

Geometrical model

The volumes of the attenuating bodies are defined by using quadratic surfaces. They are used due to their nice mathematical properties and justified by the fact that a vast amount of geometries in industry actually are quadratic. Quadratic surfaces include a large palette of geometries e.g. planes, spheres and cylinders. Following closely Bielajew[8] which presents quadratic surfaces and their solutions with a general line in a straight forward vector algebraic formalism, a geometrical kernel has been implemented.

A body is defined as a set of surfaces together with their normals (set to point away from the body interior). Then a cylinder and 2 planes, as in figure 1, enables the definition of a short piece of a wire. All bodies have a unique integer body id (bid), used to decide which body a given spatial point is to belong to when more than one body is possible.

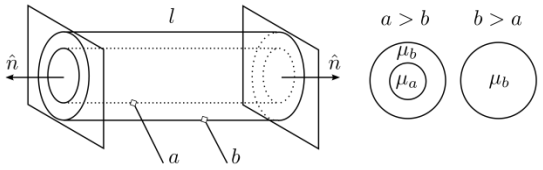

Figure 1. Illustration of a geometry built with cylinders where letters a and b indicate body id. If $\mu_a=0$, $\mu_b>0$ and a>b it will describe a hollow pipe of length l.

The algorithm calculates, for each ray starting point and direction, the intersections with each surface[8]. The effective attenuation path in equation 1 can then be deduced by summation of all these parts. General 3D rotations are handled by initially rotating all the planes, cylinder axes, points in planes and center points using Euler angles.

Weld model

Typical welds addressed within this project are groove laser welds which fulfill general weld specifications. A parameterized weld geometry has been derived for the geometry kernel. Two different cases are considered, convex (main bead is sticking out) and concave (main bead is a groove).

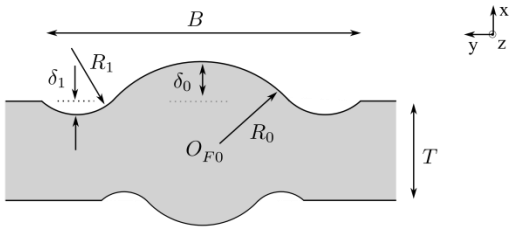

Figure 2. Weld geometry overview indicating some of the input and output parameters.

The following input parameters are defined.

δ_1	Depth/height of undercut > 0
δ_0	Depth/height main bead > 0
O^y_{F0}	Center point for main bead
B	Width of whole weld
T	Plate thickness
R_{F1}	Radius of undercut beads

Typical values for the radii on undercut beads and main bead is $\gtrsim 0.25$ mm. The width of the whole weld is at the order of 5 mm and depth/height of undercuts and main beads ~ 1 mm. Face and root side is changed for source side (SS) and detector side (DS), relating the surfaces to the x-ray setup instead.

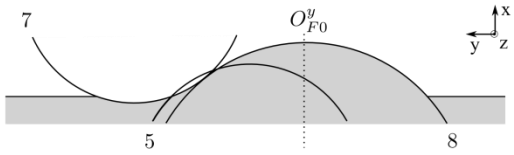

Figure 3. Weld geometry built using five cylinders, shaded regions are attenuating. Only 3 cylinders are drawn due to symmetry. The cylinders are cut using simple planes with their normals in ±x directions. Numbers indicate the arbitrary offset body ids.

Detector model

The detector types that are intended to be modeled within this project are both digital direct and indirect flat panels. Unlike the geometrical model of the weld the detector parameters doesn't need to be invertible. The signal is

assumed to be proportional to the energy that impinges the detector. The detector is modeled as consisting of conventional isotropic Gaussian point spread functions[9] (PSF) with standard deviation *GAUSTD*. In figure 4 an overview can be seen where it is clear that for SUBPXL>1 the detector samples intensity from a scalar field with higher resolution.

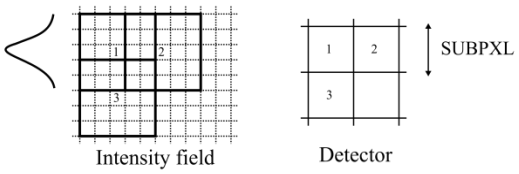

Figure 4. Center points of detector kernels of size 5 intensity pixels indicated by destination detector pixels by numbers. Intensity grid is indicted with dotted lines.

The implementation

The simple radiograph generator (SRG) kernel is written in Fortran 95 code. Input into the kernel is a parameter file defining the geometry and the output consists of a 16 bit TIFF radiograph. A verification of the geometrical definition can be generated and viewed in any VTK compatible reader.

Scattered and direct radiation simulation results

The validation of the x-ray attenuation model and the geometrical kernel has been done using the simulation software PENELOPE[1]. PENELOPE is a simulation code package using Monte Carlo methods for simulating coupled electron-photon-positron transport. Photon interactions of interest include Rayleigh scattering, Compton scattering and photoelectric absorption. Higher order terms from photoelectric excited electrons interacting and resulting in more photons are also of interest but lumped together as one whole. PENELOPE has been extensively verified experimentally[1,10,11]. If the non-linear attenuation contributions are negligible and the linear approximation model used here is consistent with the results of PENELOPE in the limit of linear attenuation, then the model and implementation proposed will be considered validated.

The PENELOPE code has been modified to split the signal into photons hitting the detector with no change in energy or angle (Primary radiation) and those with angle change and/or energy loss, Rayleigh- and Compton- scattered (Secondary radiation). Newly created photons by e.g. secondary electrons are also separated. The build-up factor[12] (BUF) is then calculated from simulations to verify the correctness of the signal splitting.

The detector output is assumed to be proportional to total energy impinging on it. Further it is modeled as ideal, i.e. the energy is integrated in an array and photons are stopped at the first interaction place in the detector.

In PENELOPE cutoff energies for electrons and photons can be specified to define when to consider them absorbed in the object. The photon absorption energy can be related to the mean free path (MFP) at that energy and the change in the detector signal which that energy would result in compared to source energy photons. It was found that setting the cutoff to 3±2 keV for the photons altered the final BUF some 1 %. With a x-ray source of 100 keV, the 6 keV scattered photon would only contribute 6 % to the detector signal compared to a primary photon. As can be seen in table 1, at 10 keV, the MFP in Ti is approximately 0.02 mm << most characteristic lengths in the setup. Thus, they will not reach

far in terms of the characteristic lengths of the setup before yet another interaction occurs.

Energy [keV]	10	40	100	200	300
μ [1/mm]	50.3	1.006	0.124	0.060	0.047
mfp [mm]	0.02	1.0	8.1	16.7	21.3

Table 1: Linear attenuation coefficients[1] for Ti used in simulations. Also shown is MFP given by μ^{-1}.

It was also verified that the total energy carried by new photons created in the object and reaching the detector was typically three orders of magnitude less than the contributions from Compton and Rayleigh scattered photons. Thus the electron absorption cutoff was set to 50 keV by verifying changes around this number to contribute considerably less to the BUF than the photon absorption cutoffs.

The BUF was verified to follow well known scaling laws[12] i.e. an increase with increased thickness and a decrease with increased energy.

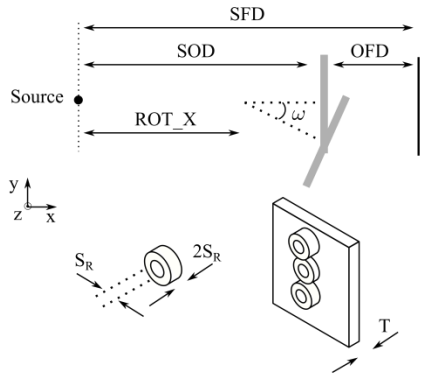

Figure 5. Drawing of the geometry used in the validation (Ti). The object used for the validation corresponds to a step-hole IQI similar to CEN Standard EN-462-2(1994).

Parameter	Range	Units
Source energy	40,100,200,300	keV
OFD	5,15,25,60	mm
T	1,2,4.5,5,8	mm
SFD	400,600,800	mm
ω	0,7.5,15	Degrees
ROT_X	SOD, SOD-50mm	mm
IQI Set Radi (S_R)	{2.5,0.4,1.0},{3.15,1.0,1.6}	mm

Table 2: Parameter ranges for validation simulation sets. See table 1 for μ(Energy)*. Different combinations of the parameters were combined using design of experiment methods.*

The simulations are run long enough in order to confirm a convergence of the BUF to less than approximately 1 %. However, decent statistics is also needed to get the scattered profiles above the noise levels. Typically ~10^9 number of source photons are used for the 1024x1024 pixel detectors.

The conclusion is that within the specified limits in table 2, with the exceptions on main energies to be >40 keV and *OFD* $\gtrsim 20$ mm, the secondary radiation contribution is negligible, see figure 6. The inhomogeneties in the scattered signal are small compared to the primary radiation signals. As expected, the inhomogeneities increase with the width of the hole and cannot be seen at the 2 mm hole in the middle. Because of this they are limited to low spatial frequency behavior. Even in the worst case scenario, figure 6a, the scattered profile is verified not to distort the spatial relations compared to the linear attenuation part.

	OFD [mm]	T [mm]	Source energy [keV]
a	5	8	100
b	25	8	100
c	15	5	200

Table 3. Parameter overview for simulations shown in figure 6. Common to all is a SFD of 600 mm and IQI step-hole set {3.15,1.0,1.6} mm.

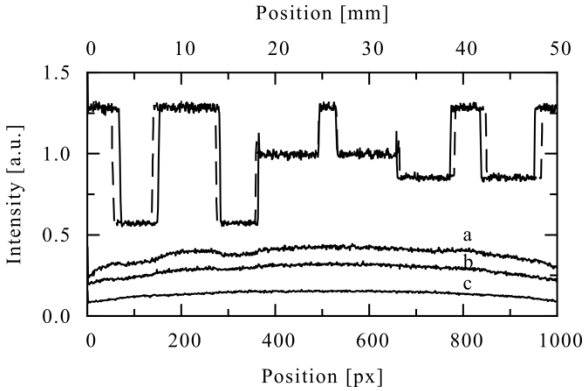

Figure 6. Intensity line profiles of width 1 pixel. Low intensity lines represent scattered radiation and solid/dashed lines at higher intensities are primary radiation for a/b where c is omitted since it is similar and just in between. See table 3 for details.

Validation of the model and its implementation

In this part the model is verified to give the same results using PENELOPE in the limit of linear attenuation. The limit is taken simply by discarding secondary radiation part of the signal and setting absorption energies to just below the source energy. A 2 dimensional nelder mead minimizer implementation[13] was included in the code to minimize the difference between PENELOPE radiograph PEN and the SRG radiograph defined as

$$\sum \Delta = \sum |PEN - k \cdot SRG|,$$

where the sum are over the 2D matrix representing the detector and the scalar k is one of the minimizing variables, the other being μ. Both variables converged with the same sum of absolute deviations within more or less machine precision compared to keeping attenuation fixed and sweeping the scale k. This indicates that the model is able to generate synthetic radiographs that are enough "realistic" and can hence later on be applied in e.g. a calibration procedure of a system.

The same geometrical setup was used as in the previous section. Also the parameter ranges as given in table 2 were used for the screening simulations. The *OFD* of 5 mm is though excluded since it is at the border of model validity.

The deviation $\sum\Delta$ can be related to the noise level in the PENELOPE radiographs which is approximated over a sub region of total N_{total} number of pixels according to

$$\sum PEN \approx \frac{N_{total}}{N} \sum_{i}^{N} |PEN_i - \langle PEN \rangle|,$$

where $\langle\rangle$ denote average. Assume that the deviation is due to some error terms E in SRG and noise in PEN signal and that they are separable according to

$$\sum \Delta = \sum PEN + \sum |E|.$$

This leads to the following approximate solution for the SNR of the error

$$SNR \approx \frac{\left(\frac{\sum \Delta}{\sum PEN} - 1\right)}{A},$$

where A is the ratio of signal area to total area. Typical deviations of the sum ratio, when keeping attenuation constant in the minimizing procedure, can be seen

in figure 7 which indicate agreement down to noise level.

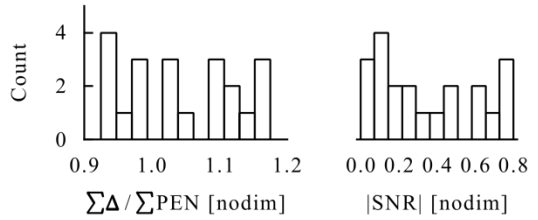

Figure 7. Distribution of $\sum\Delta/\sum PEN$ for the simulation. Also shown is the equivalent approximated SNR, where the area of the signal is approximated by measuring areas in the radiographs and range from 0.2 to 0.27 of total area.

Finally the direct comparison of SRG and PENELOPE radiographs can be seen in figure 8 which indicate good agreement.

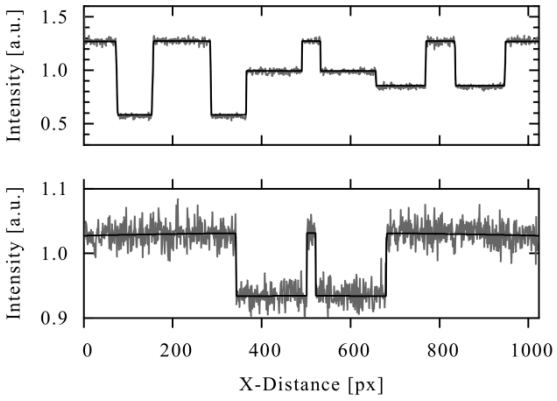

Figure 8. Some worst case (top) $(\sum\Delta)/(\sum PEN) = 1.15$ *and typical* $(\sum\Delta)/(\sum PEN) = 1.03$ *at (bottom) intensity profiles where gray signal is PENELOPE and solid one is scaled SRG. In the (top) SFD=600 mm and in the (bottom) case SFD=400 mm.*

The detector model is evaluated in terms of its resolution which is measured using modulation transfer function (MTF) formalism[14]. The MTF is the normalized modulus of the Fourier transform of the line spread function (LSF). Since the PSF of the detector is modeled as a Gaussian, the theoretical MTF for the detector system is given by

$$MTF(k) = a\left(e^{-2\pi k^2\sigma^2}\right)^2,$$

where a is a normalizing constant and σ is the standard deviation and k the frequency in cycles/mm. A standard method to evaluate MTFs of x-ray systems[12] is to expose a sharp edge of an high attenuating object. The MTF is retrieved by taking the first derivative in the direction perpendicular to the edge followed by the Fourier transform. The model is verified to agree well with the theoretical MTF, average deviations less than 1 % and maximum at 5 %. It is also compared with the MTF of a real radiograph in figure 9.

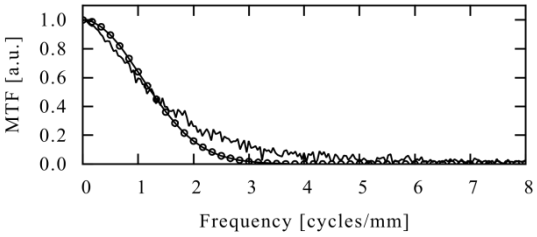

Figure 9. MTF for the simulation is indicated with round markers, compared with real radiographs MTF taken with Hamamatsu C7921CA-02 digital direct flat panel detector. The agreement is fairly good, for the hit-and-miss simulation set with SUBPXL 1 pixel, GAUSTD 3 pixel, kernel size (GAUPXL) 19 pixel, μ=0.1/mm, SFD 370 mm and OFD 100 mm.

Coarse length scale removal using wavelets

The radiographs will need to be segmented as a pre-processing stage for computerized pore detection. It will be favorable to separate the information in coarse scale (weld geometry and scattered radiation) and fine scale (pore defects and quantum noise) parts. This approach is also valuable when performing manual inspection of digital radiographs. The human vision system can at optimal conditions discriminate 700-900 gray value levels[2] which implies that often only one pore at a time can be identified in a radiograph.

The wavelet transforms has the capability to identify and separate different scales in e.g. radiographs[3]. Another but still wavelet based approach has been utilized in this paper. A fine-scale-pass filter procedure has been implemented using existing code[15]. It follows closely Mallat MRA[4,5] where the original signal is reconstructed using one wavelet level and one orientation of the coefficients in the 2D matrix at a time. The signal is summed up in the end consisting of all levels at higher levels than some threshold K, i.e. all fine-scale information above some level K is kept. It should be noted this filters out information based on its spatial dimensions in the radiograph, which might not necessarily coincide with each objects real physical length scales.

The procedure has been tested on a small set of radiographs generated using the weld geometry, described previously, containing 2 pores of different sizes. Main parameters swept out so far is the threshold level K and filter order/size for Daubechies and Symlet wavelet filters. There is an optimum place in parameter space with regard to signal to noise ratio in the resulting image, see figure 10.

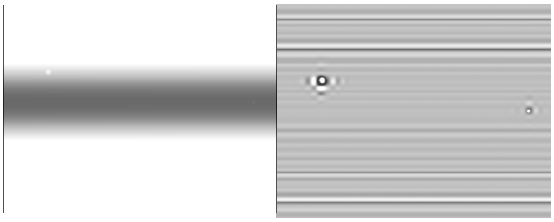

Figure 10. Synthetic radiograph (1024x1024 pixel) of a typical weld and its wavelet filtered version with K=7 using a Daubechies filter of order 14. The left is brightness-contrast optimized for showing both pores at the same time, and the right image is optimized for showing also the none-pore noise.

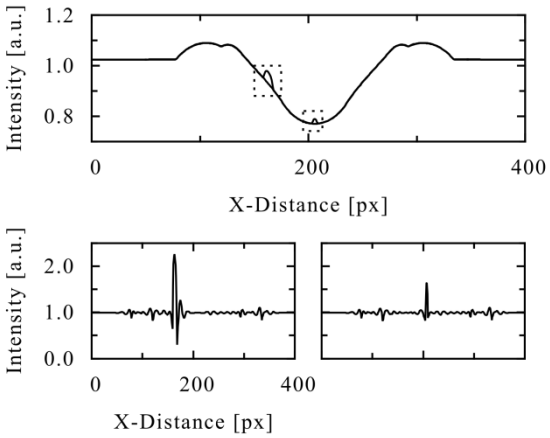

Figure 11. Vertical intensity line profiles of width 1 pixel from image in figure 10. Top) unfiltered profiles with pores indicated by dotted rectangles, profiles plotted on top of each other. Bottom) profiles from the filtered image with SNR≈15, Left) big pore and Right) small pore.

In figure 11 the line profiles clearly indicate that the none-pore noise is much less in magnitude in the filtered image. It is by this revealed that even a direct binarization, using crude thresholding, will single out the pores in this special case.

Conclusions

A model and implementation of a nondestructive testing (NDT) x-ray setup for thin groove welds in Titanium is presented. The model is found to agree well with an already experimentally verified general purpose electron and photon transport simulation package for a limited set of geometries.

The model has then been used to evaluate and implement the first steps in a digital filter chain heading towards a computerized spherical pore defect positioning procedure. Initial simulations verify an already known wavelet filtering procedure to success in

removing coarse scale intensity variations in the radiographs.

Next step is to further exploit other factors influence on the wavelet filtering, e.g. weld geometry sizes, object rotations and so on. Another important step is to implement noise terms.

Acknowledgments

The financial support by the Swedish National Aeronautical Research Program (NFFP) is gratefully acknowledged. We are also grateful to Volvo Aero Corporation for providing specifications and the industry point of view.

References

[1] F. Salvat, J. M. Fernandez-Varea and J. Sempau, "PENELOPE-2008: A Code System for Monte Carlo Simulation of Electron and Photon Transport", OECD ISBN 978-92-64-99066-1 (2008) NEA
[2] T. Kimpe and T. Tuytschaever, "Increasing the Number of Gray Shades in Medical Display Systems - How much is Enough?", Journal of Digital Imaging 20 422-432 (2007)
[3] H. Wirdelius and L. Hammar, "Modelling of a high resolution digital radiographic system and development of a filtering technique based on wavelet transforms", NDT&E International, 37 73-81 (2004)
[4] S. Mallat, "Wavelets for Vision", Proceedings of the IEEE 84 604-614 (1996)
[5] S. Mallat, "A Theory for Multiresolution Signal Decomposition: The Wavelet Representation", IEEE Transactions in Pattern Analysis and Machine Intelligence 11 674-693 (1989)
[6] G. R. Tillack, C. Nockemann and C. Bellon, "X-ray modeling for industrial applications", NDT&E International 33 481-488 (2000)
[7] D. Tucker, G. Barnes and D. Chakraborty, "Semiempirical model for generating tungsten target x-ray spectra", Med. Phys. 18 211-218 (1991)
[8] A. Bielajew, "HOWFAR and HOWNEAR: Geometry Modeling for Monte Carlo Particle Transport", Available from http://irs.inms.nrc.ca/publications/reports/ (1996) IRS
[9] S. Jeon, G. Cho, Y. Huh, S. Jin and J. Park, "Determination of point spread function for a flat-panel X-ray imager and its application in image restoration", Nuclear Instruments and Methods in Physics Research A 563 167-171 (2006)
[10] J. Sempau, J. M. Fernandez-Varea, E. Acosta and F. Salvat, "Experimental benchmarks of the Monte Carlo code PENELOPE", Nuclear Instruments and Methods in Physics Research B 207 107-123 (2003)
[11] J. Baro, M. Roteta, J. M. Fernandez-Varea and F. Salvat, "Analytical Cross Sections for Monte Carlo Simulation of photon transport", Radiat. Phys. Chem. 44 531-552 (1994)
[12] R. Halmshaw, "Industrial Radiology, Theory and practice", (1995) Springer
[13] Burkhardt, J. (2011). [Software]. Available from http://people.sc.fsu.edu/~jburkardt/f_src/asa047/asa047.html
[14] J. C. Dainty and R. Shaw, "Image Science, principles, analysis and evaluation of photographic-type imaging processes", (1974) Academic Press
[15] D. Donoho, A. Maleki, M. Shahram, (Version 850) (2011) [Software]. Available from http://www-stat.stanford.edu/~wavelab/